Changes in Diffuse Optical Tomography Images During Early Stages of Neoadjuvant Chemotherapy Correlate with Tumor Response in Different Breast Cancer Subtypes

Mirella L. Altoe[1], Kevin Kalinsky[2], Alessandro Marone[1], Hyun K. Kim[1], Hua Guo[3], Hanina Hibshoosh[3], Mariella Tejada[2], Katherine D. Crew[2,4], Melissa K. Accordino[2], Meghna S. Trivedi[2], Dawn L. Hershman[2,4], and Andreas H. Hielscher[1]

ABSTRACT

Purpose: This study's primary objective was to evaluate the changes in optically derived parameters acquired with a diffuse optical tomography breast imaging system (DOTBIS) in the tumor volume of patients with breast carcinoma receiving neoadjuvant chemotherapy (NAC).

Experimental Design: In this analysis of 105 patients with stage II–III breast cancer, normalized mean values of total hemoglobin ($ctTHb_N$), oxyhemoglobin (ctO_2Hb_N), deoxy-hemoglobin concentration ($ctHHb_N$), water, and oxygen saturation (StO_{2N}) percentages were collected at different timepoints during NAC and compared with baseline measurements. This report compared changes in these optical biomarkers measured in patients who did not achieve a pathologic complete response (non-pCR) and those with a pCR. Differences regarding molecular subtypes were included for hormone receptor–positive and HER2-negative, HER2-positive, and triple-negative breast cancer.

Results: At baseline, $ctHHb_N$ was higher for pCR tumors (3.97 ± 2.29) compared with non-pCR tumors (3.00 ± 1.72; $P = 0.031$). At the earliest imaging point after starting therapy, the mean change of $ctHHb_N$ compared with baseline ($\Delta_{TP1}ctHHb_N$) was statistically significantly higher in non-pCR (1.23 ± 0.67) than in those with a pCR (0.87 ± 0.61; $P < 0.0005$), and significantly correlated to residual cancer burden classification ($r = 0.448$; $P < 0.0005$). $\Delta_{TP1}ctHHb_N$ combined with HER2 status was proposed as a two-predictor logistic model, with AUC = 0.891; $P < 0.0005$; and 95% confidence interval, 0.812–0.969.

Conclusions: This study demonstrates that DOTBIS measured features change over time according to tumor pCR status and may predict early in the NAC treatment course whether a patient is responding to NAC.

Introduction

Neoadjuvant chemotherapy (NAC) has emerged as the standard treatment for patients with primary operable breast carcinoma, particularly in high-risk tumors, such as triple-negative breast cancer (TNBC), HER2 positive ($HER2^+$), and highly proliferative hormone receptor–positive (HR+)/HER2-negative (HER2−) breast tumors (1). The advantages include higher rate of breast-conserving surgery, downstaging disease within the breast and axilla, and long-term clinical benefit (2, 3). Pathologic response to NAC, such as residual cancer burden (RCB), reflects overall survival and disease-free survival (4–6). RCB scores are based on pathologic measurements of tumor bed size, percentage of carcinoma cellularity (discounted for *in situ* cellularity), and nodal metastases (number and size; ref. 7). A score of 0 (RCB 0) represents pathologic complete response (pCR) and scores 1–3 (RCB I, RCB II, and RCB III, also defined as non-pCR) represent increasingly greater extents of residual invasive carcinoma, and thus, associated with poorer disease-free rates and survival rates. Predicting pCR early in the therapy may allow clinicians the opportunity to optimize treatment with the ultimate goal of improving pCR rates, and ultimately better outcomes, as well as avoiding toxicity from ineffective therapies.

This study adds to the body of evidence reported for diffuse optical imaging methods applied to breast cancer treatment response. Our findings complement and extend previous smaller studies conducted from 2007 to 2018 (8–18) that have identified optical-based imaging markers correlated to pCR at different timepoints throughout NAC. In a meta-analysis study (19), Liu and colleagues demonstrated that diffuse optical tomography (DOT) has clinically acceptable predictive values. Their results show that the best single predictor of therapeutic response was *ctHHb* (83% sensitivity and 100% specificity) after 1 week posttreatment. In 2011, a multicenter study (20) showed changes from baseline to mid-therapy predict pCR in women undergoing NAC ($n = 34$). Later, a second publication (21), using the same patient cohort, found that tissue oxygen saturation measured within 10 days of NAC was a predictor of pCR. Therefore, our clinical study represents one of the larger studies ($n = 89$) of this topic to date and uses more modern criteria for pathologic response, both pCR status and RCB scores.

[1]Departments of Biomedical Engineering, New York University Tandon School of Engineering, Brooklyn, New York. [2]Division of Hematology/Oncology, Department of Medicine, Columbia University Irving Medical Center, New York, New York. [3]Department of Pathology and Cell Biology, Columbia University Irving Medical Center, New York, New York. [4]Department of Epidemiology, Columbia University Irving Medical Center, New York, New York.

Note: Supplementary data for this article are available at Clinical Cancer Research Online (http://clincancerres.aacrjournals.org/).

Corresponding Authors: Mirella L. Altoe, Department of Biomedical Engineering, Clinical Biophotonics Laboratory (CBL), New York University, 433 1st Avenue, New York, NY 10010. Phone: 917-698-3480, E-mail: mla9973@nyu.edu; and Andreas H. Hielscher, Department of Biomedical Engineering, Clinical Biophotonics Laboratory (CBL), New York University, Tandon School of Engineering, 6 Metro Tech Center, Brooklyn, NY 11201. Phone: 134-7439-0484, E-mail: ahh4614@nyu.edu

Clin Cancer Res 2021;27:1949–57

doi: 10.1158/1078-0432.CCR-20-1108

Translational Relevance

This study demonstrates that imaging features generated by a diffuse optical tomography breast imaging system may predict early in the neoadjuvant chemotherapy treatment course whether a breast carcinoma will achieve pathologic complete response, and the need to stratify chemotherapy response prediction according to tumor subtype.

In summary, the purpose of this study was to investigate the change of quantitative measurements of tissue functional components, such as hemoglobin concentration, measured with DOT breast imaging system (DOTBIS) in the tumor region of patients receiving NAC. We hypothesize that hemoglobin values are modifiable at different timepoints along with the NAC regimen, and their changes after 2–3 weeks are associated with pCR and are dependent on breast carcinoma subtype.

Materials and Methods

Study population

According to a study by Lim and colleagues (14) and Soliman and colleagues (10), a clinically significant effect of 50% or more in the hemoglobin levels between pCR and non-pCR would be of interest. Assuming a reduction in the pCR group of approximately 30% and a 20% increase in the non-pCR group, with a two-sided significance of 0.05 and a power of 0.9, a minimum of 66 patients would be required. In this study, 105 patients with stage II—III breast cancer were prospectively enrolled in an Institutional Review Board–approved clinical protocol at Columbia University Irving Medical Center (New York, NY) between 2011 and 2019. Each patient received a taxane-based regimen. Pathologic response, as defined by Symmans and colleagues (7), was dichotomized, with pCR defined as complete absence of invasive carcinoma in the breast and lymph node(s) (ypT0/is ypN0 Mx) at the time of surgery. Menopausal status, age, and body mass index (BMI) were recorded in the patient's electronic medical record and retrieved for this work. This study was compliant with the Health Insurance Portability and Accountability Act, and conducted in accordance with the Declaration of Helsinki. Written informed consent was obtained from all study participants.

DOTBIS measurements

We employed a steady-state DOTBIS to image the whole breast volume using near-infrared light (22–25). The data were used to calculate tissue concentration of oxyhemoglobin (ctO_2Hb), deoxy-hemoglobin ($ctHHb$), total hemoglobin ($ctHbT = ctO_2Hb + ctHHb$), and water percentage. Total measurement time varied between 6 and 8 minutes, according to breast size, in addition to 5 minutes required to set up the machine. A PDE-constrained multispectral image reconstruction code (26) created 3D image maps of ctO_2Hb, $ctHHb$, $ctHbT$, StO_2, and water. For visualization purposes only, maximum intensity projections (MIP; ref. 27) were acquired from reconstructed data volume and translated into a view plane, which can be obtained by finding the voxels with maximum intensity along a chosen axis. An automated code was designed to select the highest value in the breast quadrant defined by the tumor's distance from the nipple and the clock position entered by the user. Subsequently, a region-based image segmentation method was employed to examine neighboring pixels of the highest value point detected in the quadrant previously specified and to determine whether the proximate pixel should be added to the region considering a mask of 90%. Mean concentration values for each chromophore acquired from the tumor region were normalized by the mean values calculated from the nontumor volume, and they expressed the magnitude of tumor concentration values in respect to the nonaffected tissue. For notation purposes, the normalized feature is identified by the subscript letter N (i.e., $ctHHb_N$). Also, the normalized features for each imaging timepoint acquired after NAC initialization were standardized by the normalized values acquired at baseline (TP0). This proposed ratio directly evaluates the percentage change to the baseline values and is represented by the symbol Δ. For instance, to represent the difference between the $ctHHb_N$ measured at TP1 compared with baseline, we write $\Delta_{TP1}ctHHb_N$.

Imaging protocol

For patients ($n = 69$) receiving 12 cycles of weekly paclitaxel (T, with or without addition of carboplatin), followed by four cycles of doxorubicin and cyclophosphamide (AC) given every 2 weeks with growth factor support [T $\times$ 12/AC $\times$ 4 or cytoxan plus taxotere (T/C) $\times$ 12/AC $\times$ 4], DOTBIS measurement was acquired at six different timepoints: before starting NAC regimen (baseline), after 2 weeks of taxane infusions (TP1), after 4 weeks of taxane (TP2), at the end of the taxane regimen and before starting AC cycles (TP3), after two cycles of AC (TP4), and at the end of NAC and before surgery (TP5). For other taxane-based NAC regimens without an anthracycline ($n = 36$), the patients were imaged only three times [baseline, 2–3 weeks after the first taxane infusion (TP1), and at the end of NAC and before surgery (TP5)], as illustrated in **Fig. 1**.

Statistical analysis

Statistical analyses were computed using the statistical software program SPSS version 16.0 (SPSS). Significant difference in DOTBIS-measured levels between pCR and non-pCR groups, and RCB classes were assessed at baseline (TP0) and at the earliest timepoint after NAC (TP1). At TP0, to select the best possible subject of predictors from all the five DOTBIS features available (i.e., $ctTHb_N$, ctO_2Hb_N, $ctHHb_N$, $StO2_N$, and $Water_N$), we applied backward stepwise selection to carry out the choice of significant predictive variable by an automatic procedure. At TP1, a new set of predictors was available (i.e., $\Delta_{TP1}ctTHb_N$, $\Delta_{TP1}ctHHb_N$, $\Delta_{TP1}ctO_2Hb_N$, $\Delta_{TP1}StO2_N$, and $\Delta_{TP1}Water_N$). We also performed backward stepwise selection to identify the best predictor set for pCR and RCB classification at TP1.

Independent sample t tests were conducted to determine whether there were differences in the selected DOTBIS feature values between pCR and non-pCR groups. One-way ANOVA was necessary for comparisons of more than two groups as demanded by RCB classification. To evaluate whether a two-way interaction exists, that is, between tumor response and molecular subtypes and DOTBIS measurement values, a two-way ANOVA followed by Tukey HSD *post hoc* tests was carried out. Besides, Pearson product-moment correlation was used to assess the relationship between changes after 2–3 weeks of NAC and RCB score. For response prediction analyses, a binomial logistic regression was performed for all patients to ascertain the effects of changes in optical features after 2–3 weeks because taxane initiation (TP1) combined with tumor subtype information on the likelihood that tumor will not achieve pCR after NAC. We also extended our analysis to investigate how DOTBIS-measured values evolve across multiple imaging timepoints when we correct for pCR group classification. We used the nlme package (28) available in R to perform longitudinal multilevel mixed-effects modeling analysis. Finally, survival analysis was focused on the nonoccurrence of disease progression

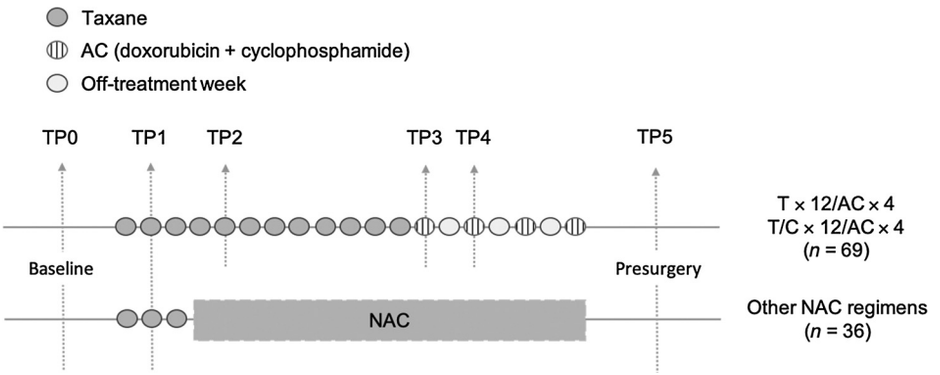

Figure 1.

Study calendar for patients receiving weekly taxane followed by AC (T × 12/AC × 4 and T/C × 12/AC × 4) and for other taxane-based NAC regimens. Patients under T × 12/AC × 4 and T/C × 12/AC × 4 therapies ($n = 69$) were imaged at baseline (TP0), 2 weeks after the first taxane infusion (TP1), after four infusions of taxane (TP2), at the end of the taxane regimen and before starting AC cycle (TP3), after two AC infusions (TP4), and at the end of NAC and before surgery (TP5; top). For other taxane-based NAC regimens without an anthracycline ($n = 36$), all patients were imaged only three times: TP0, 2–3 weeks after the first taxane infusion (TP1), and TP5 (bottom).

or recurrence. Kaplan–Meier estimates were used to compare event-free survival (EFS) between RCB classification groups and DOTBIS optical-based imaging feature (i.e., $\Delta_{TP1}ctHHb_N$). Kaplan–Meier survival curves were compared with the log-rank test. Significance was assumed at a confidence interval of 95% ($\alpha = 0.05$).

Results

Patient and tumor characteristics

From a total of 105 patients, 17 were excluded from the final analysis (Supplementary Table S1). The main reasons for exclusion were: patient withdrew from the study ($n = 4$), baseline DOTBIS measurement not collected because of instrumentation failure ($n = 8$), patient under investigational and not FDA-approved drug regimen ($n = 1$), and machine operator error ($n = 4$). One patient had bilateral breast cancer, and both tumors were added to the analysis. Therefore, results include 88 patients and 89 tumors in total. RCB scores were not available for these two tumors and another four cases. Not all the patients had their DOTBIS reconstruction available for all of their imaging timepoints due to patient declining imaging at that particular DOTBIS timepoint or machine malfunction. Overall, 82 (93%) patients had DOTBIS images successfully reconstructed at baseline (TP0), 70 (80%) patients at 2–3 weeks from taxane initiation (TP1), and 52 (59%) at the presurgical timepoint (TP5). In total, 36 did not have TP5 imaging available. The reasons for missing data were patient declined to be imaged (19/36), machine operator did not collect/save the data correctly (5/36), and data not collected because of machine under repair (12/36). Of the 58 patients who were under T × 12/AC × 4 regimen ($n = 54$) or T/C × 12/AC × 4 ($n = 4$), 46 (79%) had their data acquired and reconstructed at TP2, 43 (74%) at TP3, and 40 (69%) at TP4. Other regimens accounted for the remaining 30 patients. Twenty-two patients (25%) with $HER2^+$ breast cancer received six cycles of docetaxel, carboplatin, and trastuzumab plus pertuzumab (TCHP). Six patients (6.8%) received six cycles of cytoxan plus taxotere (T/C × 6), and one patient (1.1%) received just four cycles of cytoxan plus taxotere (T/C × 4). Finally, one patient (1.1%) received paclitaxel, trastuzumab, and pertuzumab, followed by doxorubicin and cyclophosphamide (THP/AC). Patient and clinical characteristics are summarized in **Table 1**. As summarized in **Table 1**, none of the patients enrolled in this study received an antiangiogenic agent (e.g., bevacizumab), and all breast cancer subtypes were eligible. A total of 36 tumors (40%) achieved pCR, whereas 53 (60%) were classified as non-pCR, that is, RCB > 0. **Figure 2** provides the sagittal MIP of the tumor-bearing breast ctTHb volumetric map of two 46-year-old

Table 1. Demographic and clinical characteristics for all the 88 patients (89 tumors) considered for analysis.

Patient and clinical characteristics	Number of patients	Age (mean ± SD)	BMI (mean ± SD)
Chemotherapy and targeted therapies			
T × 12/AC × 4	54	48.48 ± 11.52	29.89 ± 7.18
TCHP	22	54.00 ± 9.83	29.36 ± 9.35
T/C × 6	6	59.67 ± 12.24	30.54 ± 3.24
T/C × 12/AC × 4	4	39.25 ± 8.65	30.05 ± 2.29
T/C × 4	1	30	18.11
THP/AC	1	40	32.23
Menopausal status			
Premenopausal	52	41.65 ± 6.90	29.48 ± 7.91
Postmenopausal	35	61.63 ± 6.00	30.10 ± 6.82
Uncertain	1	56	27.16

Tumor characteristics	Number of tumors
Treatment response classification	
pCR	
RCB0	36
non-pCR	
RCBI	10
RCBII	27
RCBIII	11
RCB score not available	5
Molecular features	
$HR^+/HER2^-$	45
$HER2^+$	27
TNBC	17

Note: T × 12/AC × 4, 12 cycles of weekly paclitaxel followed by four cycles of doxorubicin and cyclophosphamide given every 2 weeks with growth factor support; T/C × 12/AC × 4, 12 cycles of weekly paclitaxel followed by four cycles of doxorubicin and cyclophosphamide given every 2 weeks with growth factor support with an addition of carboplatin to paclitaxel; T/C × 6, six cycles cytoxan plus taxotere; T/C × 4, four cycles cytoxan plus taxotere.
Abbreviation: HR, hormone receptor.

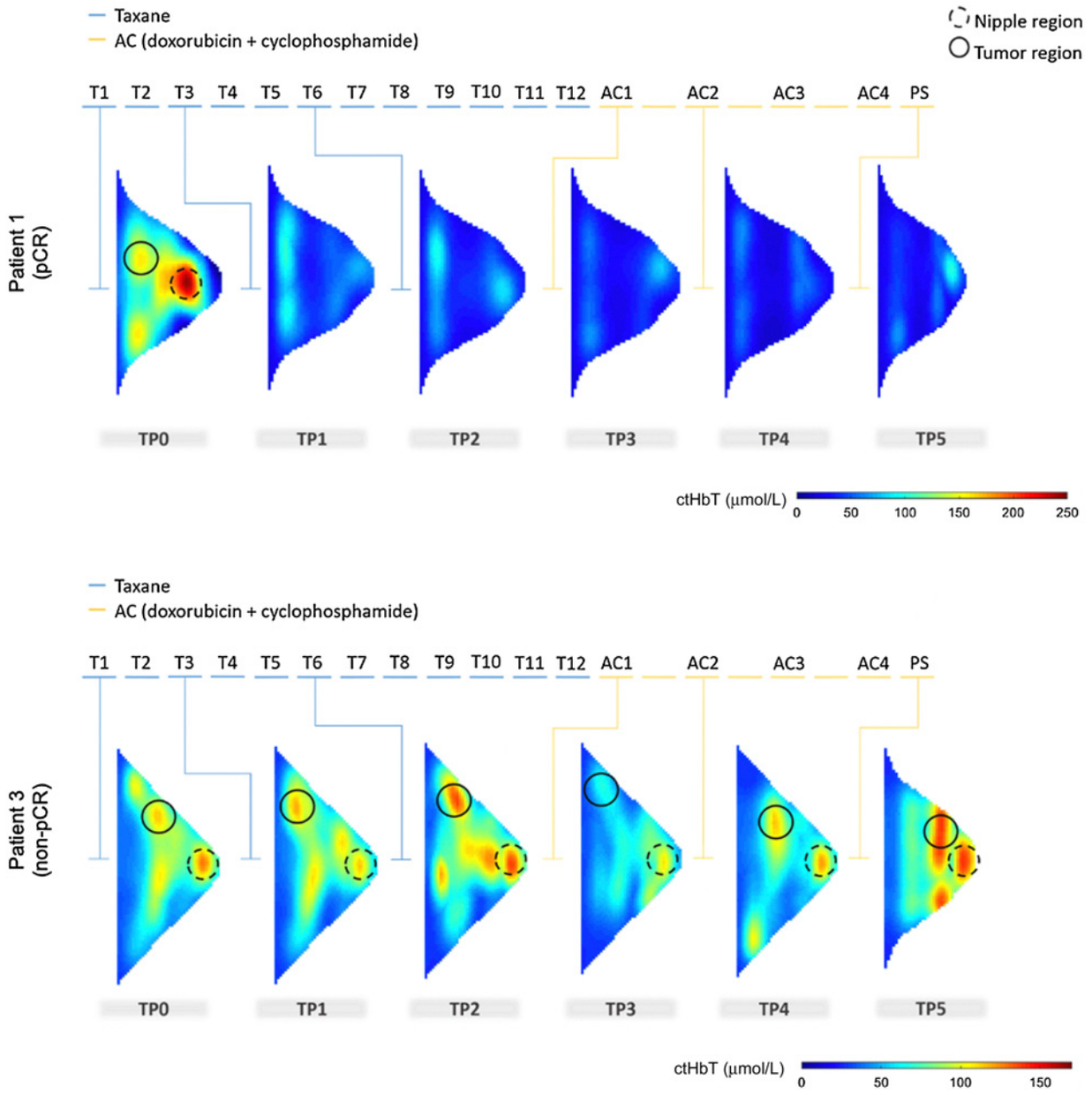

Figure 2.

Sagittal MIP of the tumor-bearing breast ctTHb volumetric map of a 46-year-old woman (patient 1) who achieved pCR after NAC for $HER2^{+}$ breast cancer (top) and a 46-year-old woman (patient 3) and $HER2^{-}$ breast cancer who was classified as RCBIII (non-pCR; bottom). NAC drug regimen protocol includes 12 cycles of weekly paclitaxel (blue) followed by four cycles of AC given every 2 weeks (yellow). DOTBIS images corresponding to baseline, before the first taxane treatment (T1), before her third and fifth taxane cycle (T3 and T5), before her first and second AC cycles (AC1 and AC2), and presurgery (PS) are arranged from left to right. The dashed circle line identifies the nipple region.

women, one pCR and another non-pCR, respectively. A full 3D *ctTHb* map is also available for both patients (Supplementary Fig. S1).

DOTBIS-measured values at baseline and tumor response to NAC

$ctTHb_N$, ctO_2Hb_N, $ctHHb_N$, $StO2_N$, and $Water_N$ values were available for all the 89 tumors. Backward stepwise selection results show that the best predictor for pCR and RCB classification at baseline was $ctTHb_N$. After computing an independent *t* test, baseline $ctTHb_N$ levels (ratio between *ctTHb* tumor values and surrounding nonaffected tissue volume) were higher for pCR tumors (3.97 ± 2.29) compared with non-pCR (3.00 ± 1.72; $P = 0.03$; **Fig. 3**, left). Additional analysis was extended to RCB score values instead of binary pCR status classification. ANOVA test results did not show a statistically significant difference in baseline $ctTHb_N$ levels between the four RCB classes ($P = 0.056$; **Fig. 3**, right).

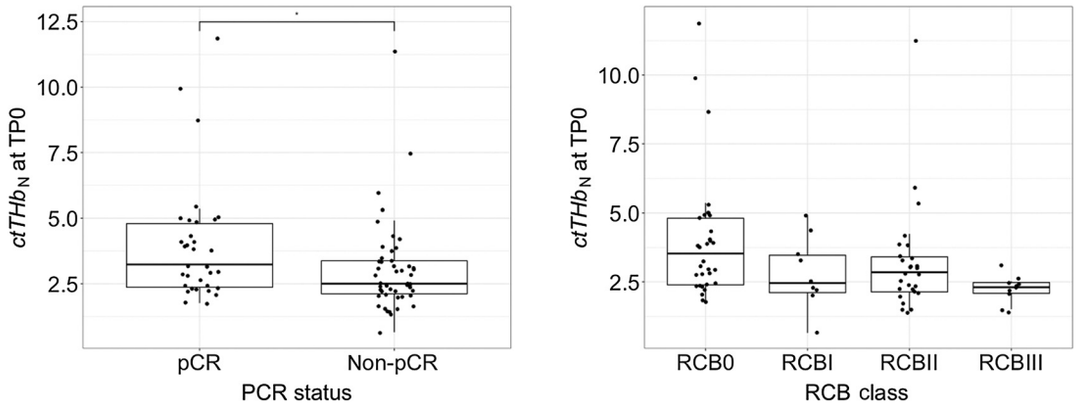

Figure 3.

Clustered box plot of $ctTHb_N$ for both pCR ($n = 37$) and non-pCR groups ($n = 52$; left). Clustered box plot of $ctTHb_N$ for the four different RCB classes: RCB0 ($n = 37$), RCBI ($n = 10$), RCBII ($n = 27$), and RCBIII ($n = 11$; right). There was a statistically significant difference between pCR and non-pCR tumors at baseline ($P = 0.03$).

A two-way ANOVA was conducted to examine the effects of pCR status (pCR and non-pCR) or RCB classification (RCB0, RCBI, RCBII, and RCBIII), and molecular subtype ($HER2^+$, TNBC, $HR^+/HER2^-$) on baseline $ctTHb_N$ levels. Sample size and mean baseline $ctTHb_N$ for all three molecular subgroups according to pCR and RCB classification are provided in the Supplementary Data (Supplementary Table S2). There was a statistically significant interaction between the effects of pCR status and molecular subtype on $ctTHb_N$ levels at TP0, before starting NAC [$F(2,77) = 3.450$; $P = 0.037$]. Tukey HSD *post hoc* tests were carried out. There was no statistically significant difference in baseline $ctTHb_N$ values between pCR and non-pCR within the same molecular subgroup. The only significant difference was between baseline $ctTHb_N$ values for TNBC pCR tumors (5.15 ± 2.26) and $HR^+/HER2^-$ non-pCR tumors (1.60 ± 0.75; $P = 0.46$). No statistical significance was reported when analyzing the effects of RCB classification and molecular subtype [$F(4,67) = 1.242$; $P = 0.30$].

DOTBIS-measured values at the earliest timepoint and tumor response to NAC

$\Delta_{TP1}ctHHb_N$ was the best predictor for pCR classification at the earliest timepoint (TP1) after performing a backward stepwise selection. $ctHHb_N$ levels after one dose of taxane for pCR tumors (0.87 ± 0.61) were significantly lowered compared with non-pCR (1.23 ± 0.67; $P < 0.0005$; **Fig. 4**, left). A one-way ANOVA test was conducted to investigate significant differences in $\Delta_{TP1}ctHHb_N$ levels between the four RCB classes. There was a significant effect of RCB classification on the change of $ctHHb_N$ levels after 2–3 weeks under NAC ($\Delta_{TP1}ctHHb_N$) at the $P < 0.0005$ level for the four RCB classes [$F(3,62) = 10.29$; $P < 0.0005$]. *Post hoc* comparisons using the Tukey HSD test indicated that the mean $\Delta_{TP1}ctHHb_N$ value for RCB0 tumors (0.782 ± 0.293) was significantly different than the RCBI tumors (1.18 ± 0.244; $P = 0.017$), RCBII tumors (1.21 ± 0.290; $P < 0.0005$), and RCBIII tumors (1.22 ± 0.395; $P = 0.002$; **Fig. 4**, right).

A two-way ANOVA was conducted to investigate pCR (pCR and non-pCR) or RCB classification (RCB0, RCBI, RCBII, and RCBIII), and molecular subtype on the ratio of change in $ctHHb_N$ levels after 2–3 weeks under NAC ($\Delta_{TP1}ctHHb_N$). Sample size and mean $\Delta_{TP1}ctHHb_N$ for all three molecular subgroups according to pCR and RCB classification are provided in the Supplementary Data (Supplementary Table S4). There was a statistically significant interaction between the effects of pCR status and molecular subtype on $\Delta_{TP1}ctHHb_N$ levels [$F(2,63) = 6.381$; $P = 0.003$]. Tukey HSD *post hoc* tests were carried out. For $HR^+/HER2^-$ pCR tumors, $\Delta_{TP1}ctHHb_N$ levels were statistically significant lower (0.857 ± 0.309) than $HR^+/$

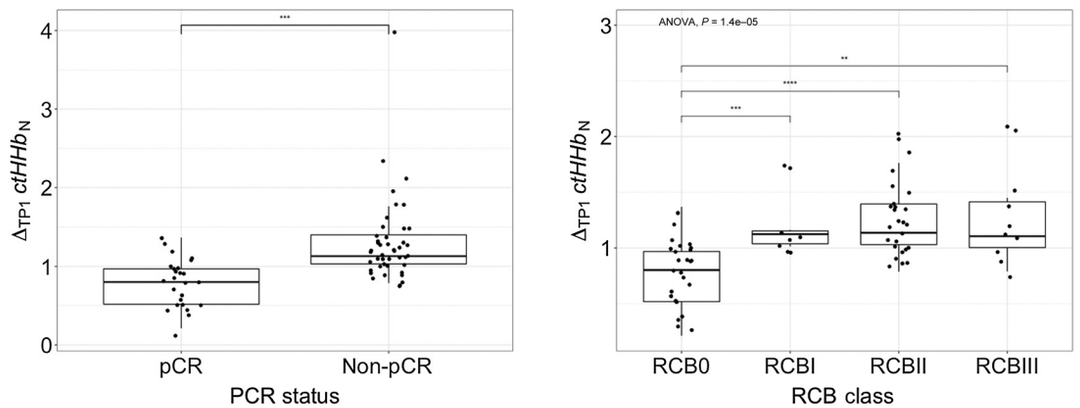

Figure 4.

Clustered box plot of $\Delta_{TP1}ctHHb_N$ for both pCR ($n = 25$) and non-pCR groups ($n = 44$; left). Clustered box plot of $\Delta_{TP1}ctHHb_N$ for the four different RCB classes: RCB0 ($n = 25$), RCBI ($n = 7$), RCBII ($n = 25$), and RCBIII ($n = 9$; right). There was a statistically significant difference between pCR status ($P < 0.0005$) and RCB0 classes ($P < 0.0005$).

HER2$^-$ non-pCR subgroup (2.33 ± 1.55; $P < 0.0005$). There was no other significant difference between pCR and non-pCR tumors within TNBC or HER2$^+$ molecular subgroups. No statistical significance was reported when analyzing the effects of RCB classification and molecular subtype [F (4,56) = 1.100; $P = 0.35$). Pearson product-moment correlation was run to assess the relationship between $\Delta_{TP1}ctHHb_N$ and RCB scores. There was a statistically significant moderate positive correlation between changes in $ctHHb_N$ after 2–3 weeks of NAC and RCB score after chemotherapy [$r(66) = 0.448$; $P < 0.0005$; Supplementary Fig. S2].

Finally, $\Delta_{TP1}ctHHb_N$ combined with HER2 status was used as a two-predictor logistic model. The logistic regression model was statistically significant [χ^2 (2) = 35.510; $P < 0.0005$]. The model explained 55.1% (Nagelkerke R^2) of the variance in pCR status and correctly classified 75.4% of cases. According to the model, the log of the odds of a patient not responding to NAC was positively related to $\Delta_{TP1}ctHHb_N$ ($P = 0.001$) and HER2 status ($P = 0.024$). In other words, the higher the $\Delta_{TP1}ctHHb_N$ ratio, the less likely it is that the patient will have a pCR. Given the same $\Delta_{TP1}ctHHb_N$ value, patients with HER2$^+$ breast cancers were 4.8 times more likely to have a pCR than those with HER2$^-$ tumors. ROC of the proposed logistic regression model indicated an excellent level of discrimination employing the criteria defined by Hosmer and colleagues. Sensitivity was 95.5%, specificity was 64%, with a positive predictive value of 81.8% and a negative predictive value of 64%. The AUC was 0.891 ($P < 0.0005$), with 95% confidence interval (0.812–0.969).

DOTBIS-$ctHHb_N$ across NAC: three- and six-timepoint studies

Given that $ctHHb_N$ was the best predictor after one cycle of taxane, we also evaluated the time evolution of this feature across other NAC imaging timepoints.

Three-timepoint imaging cohort

Thirty-four tumors were under a three-timepoint imaging schedule, 17 pCR and 17 non-pCR. By applying multilevel modeling and setting up $ctHHb_N$, as the dependent variable, and pCR classification and molecular subtype as predictors in the model, we evaluated the potential difference in time evolution between the pCR groups. The difference in changes from baseline was significant between pCR and the non-pCR groups at both TP1 (4.25 ± 1.53; = 0.0085) and TP5 (6.83 ± 2.10; $P = 0.0024$). This indicates that the mean $ctHHb_N$ over time differed significantly between pCR groups. Mean $ctHHb_N$ value was different between molecular subtype groups at baseline ($P = 0.0451$), but $ctHHb_N$ changes across time were not statistically significantly different according to the molecular subgroup.

Six-timepoint imaging cohort

For the six-timepoints longitudinal cohort, 55 breast cancer tumors were included, 20 had pCR and 35 were classified as non-pCR. From multilevel modeling results, changes in $ctHHb_N$ levels compared with baseline (TP0) values were statistically significantly different between pCR and non-pCR at TP1 (1.93 ± 0.40; $P < 0.0005$), TP2 (2.05 ± 0.82; $P = 0.0132$), TP4 (2.72 ± 0.86; $P = 0.0019$), and TP5 (2.64 ± 0.89; $P = 0.0036$). No significant changes over time were identified between molecular subtype groups.

EFS analysis

Recurrence and disease progression were observed in 20.4% ($n = 18$) of the patients, including 13 patients presented with distant metastasis. The most common metastasis sites included lungs ($n = 4$), bone ($n = 2$), and brain ($n = 2$). Five patients (5.7%) did not survive the 5-year follow-up period, and all of them had disease progression or recurrence before death. Kaplan–Meier survival curve analysis was performed (**Fig. 5**, top), and RCB classification was associated with worse EFS (log-rank test, $P = 0.0015$). Also, we observed worse EFS in patients with an increase in $ctHHb_N$ levels after 2–3 weeks NAC compared with baseline values (**Fig. 5**, bottom), but the difference was not significant (log-rank test, $P = 0.11$).

Discussion

Predicting pCR early in the course of therapy is of great clinical interest in order to avoid ineffective treatment. In addition, the neoadjuvant setting is promising for subtype- and response-tailored trials. To identify different treatment regimens that may be more effective to be pursued, there is a clinical need of imaging markers that enable noninvasive prediction of pCR. In this study, we demonstrated that DOTBIS measured features change in accordance with pCR status after 2–3 weeks under NAC, and when combined to HER2 status could be a predictive factor for pCR. Our findings complement and extend previous smaller studies conducted from 2007 to 2018 (8, 9, 11–18, 20, 21). Giving our larger sample size ($n = 89$), and multiple imaging timepoints, we were also able to detect differences within the breast tumor subtypes. Because of sample size restriction, differences between pCR status stratified by molecular subgroups were only noticed within the HR$^+$/HER2$^-$ subgroup (pCR, $n = 10$ and non-pCR, $n = 35$). Overall, the data show a significant decrease in normalized values of *ctHHb* for patients with pCR compared with non-pCR, and such changes were noticed at the earliest imaging timepoint (TP1). The changes in *ctHHb* levels at TP1 were also moderately positively correlated to RCB scores. In addition, from the longitudinal multilevel mixed-effects results, we observed that in both three- or six-timepoint imaging studies, *ctHHb* change differed over time between pCR and non-pCR groups. When looking at the biological point of view, *ctHHb* can be attributed to tumor tissue oxygen consumption, and it is sensitive to cellular metabolism. Therefore, reduction in *ctHHb* levels represents the chemotherapeutic-induced changes in the tumor microvasculature: lower *ctHHb* values associate with the reduction in tumor cell proliferation, and consequently in oxygen consumption, and might provide tumor response prediction to NAC. However, different from previous publications (15, 29), our data did not show any significant differences in changes of ctO_2Hb_N levels according to pCR status. It is possible that ctO_2Hb_N, which is more representative of vascular supply and oxygen delivery, could be less variable to meet the demands of diminished cellularity because of cell death of the tumor tissue. However, a larger study is necessary to confirm the actual biochemical significance of ctO_2Hb_Nvariation across NAC in comparison with *ctHHb*.

In addition, at baseline, normalized *ctHHb* levels ($ctHHb_N$), calculated from both the tumor volume and nonaffected tissue, differentiate pCR status. Tumors that achieved pCR were characterized by higher $ctHHb_N$ levels, which represent tumor volume values almost four times higher than the surrounding healthy tissue. In contrast, $ctHHb_N$ levels were lower for non-pCR tumors. DCE-MRI findings (30–34) have also observed a consistent pretreatment differentiation between pCR and non-pCR radiomics. Braman and colleagues demonstrated that pCR tumors were characterized by increased homogeneity features within the tumor and decreased expression of gradient entropy features at the perimeter compared with non-pCR tumors (31). For that study, the authors hypothesize that these specific

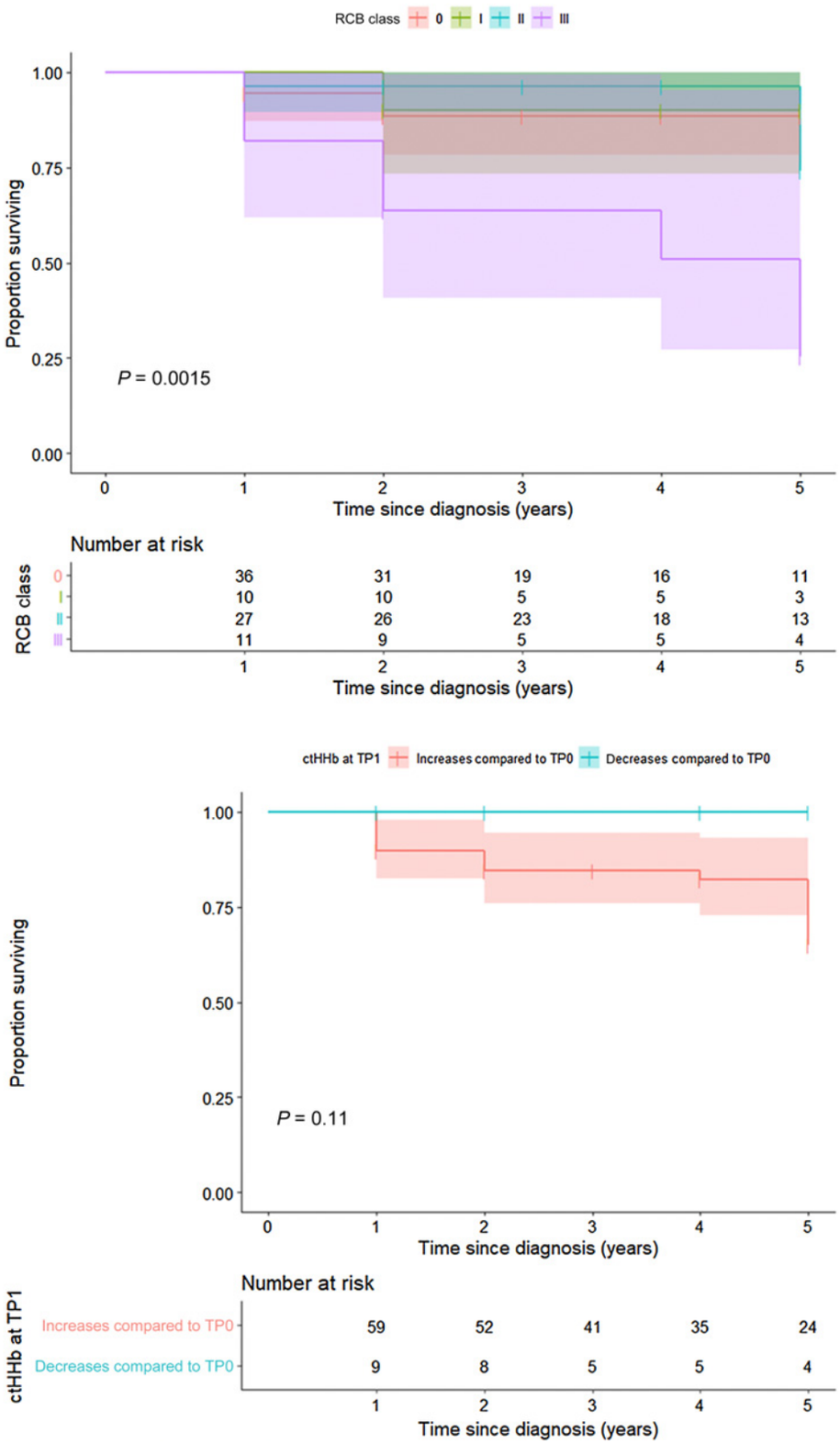

Figure 5.

Kaplan–Meier survival curves according to RCB classification (top) and change in $ctHHb_N$ levels (bottom) after 2–3 weeks under NAC ($\Delta_{TP1}ctHHb_N$).

radiomics expressions could be correlated to the fact that non-pCR tumors are known for containing intermingled tumor cells, necrosis, and sclerosis besides a high angiogenic activity within and surrounding the non-pCR tumors. On the other hand, pCR tumors are characterized by intratumoral volume containing densely packed stromal tumor-infiltrating lymphocytes (TIL). High levels of TILs have been associated with improved outcome and increased response to NAC in both $HER2^+$ and TNBC (34, 35).

To our knowledge, this is the first work to investigate the effect on a 5-year window prognosis by comparing patients that had a decrease in hemoglobin tumor levels after 2–3 weeks under NAC with those in whom it increased. Although we observed a tendency toward a correlation of $\Delta_{TP1}ctHHb_N$ with EFS, we believe that due to the sample size limitation and the maximum follow-up of 5 years (mean follow-up of 3.4 years), we could not obtain statistical power to detect clinically relevant differences based on DOTBIS features. Further studies with a larger sample size and a longer follow-up period are warranted to assess the prognostic factors of disease recurrence in patients receiving NAC using DOTBIS optical imaging features.

Our study has limitations. Patients' menstrual cycles at baseline were not uniformly reported, and, therefore, were not accounted for analyses, which could cause variation in the baseline hemoglobin measures. Tumor location selection was based on distance from the nipple and quadrant information available from the patient's radiology report. The same tumor position was assumed for all the imaging time points. Tumor values were normalized by the nontumor tissue, so any variability from inter- and intrapatient analyses could be diminished. But no additional work was done to consider the variations from different breast density groups. In addition, a larger study population may enable researchers to investigate the impact of different chemotherapy regimens and draw better conclusions regarding molecular subgroups. Finally, no data were reported for tumor sizes smaller than 1 cm, and there is no support that such technology could be used to assess changes in small tumor volumes.

In summary, we have evaluated longitudinal changes in hemoglobin values across NAC between pCR and non-pCR tumors, as well as according to RCB classification. At baseline, normalized $ctTHb_N$ total hemoglobin levels were statistically different between responders and nonresponder. Also, changes in normalized deoxy-hemoglobin values after 2–3 weeks under NAC were associated with pCR and were dependent on breast carcinoma subtype. These results confirm the potential of DOTBIS for predicting patients that would most benefit from personalized therapeutic approaches and the need to investigate chemotherapy response prediction according to tumor phenotype. If further validated on a larger set, these data could potentially be used to optimize response to NAC.

Authors' Disclosures

K. Kalinsky reported other from Eli Lilly, Pfizer, Novartis, Eisai, AstraZeneca, Immunomedics, Merck, Seattle Genetics, Cyclocel, and Grail outside the submitted work. A.H. Hielscher reported grants from Columbia | Biomedx during the conduct of the study, as well as had a patent for "digital signal processor based detection system, method, and apparatus for optical tomography" (US 7463362 B2) issued, "systems and methods for dynamic imaging of tissue using digital optical tomography" (US 9037216 B2) issued, and "interfacing systems, devices, and methods for optical imaging" (20140236003 A1) issued. No disclosures were reported by the other authors.

Authors' Contributions

M.L Altoe: Conceptualization, data curation, software, formal analysis, validation, investigation, visualization, methodology, writing–original draft, writing–review and editing. **M.S. Trivedi:** Resources, writing–review and editing. **D.L. Hershman:** Conceptualization, resources, data curation, supervision, funding acquisition, validation, investigation, project administration, writing–review and editing. **A.H. Hielscher:** Conceptualization, formal analysis, supervision, funding acquisition, validation, investigation, writing–original draft, project administration, writing–review and editing. **K. Kalinsky:** Conceptualization, resources, data curation, supervision, funding acquisition, validation, investigation, project administration, writing–review and editing. **A. Marone:** Software, visualization, methodology, writing–review and editing. **H.K. Kim:** Software, visualization, methodology, writing–review and editing. **H. Guo:** Resources, writing–review and editing. **H. Hibshoosh:** Resources, writing–review and editing. **M. Tejada:** Data curation, project administration. **K.D. Crew:** Resources, writing–review and editing. **M.K. Accordino:** Resources, writing–review and editing.

Acknowledgments

The authors thank the patients who generously volunteered their time for this study. This work was supported, in part, by a grant from Columbia | Biomedx - Biomedical Technology Accelerator and the Breast Cancer Research Foundation. Furthermore, M.L. Altoe was supported, in part, by a fellowship from CNPq/LASPAU – Brazil (207913/2014-5), and A. Marone was supported, in part, by a Personalized Medicine Fellowship of the Irving Institute for Clinical and Translational Research at Columbia University in the City of New York.

The costs of publication of this article were defrayed in part by the payment of page charges. This article must therefore be hereby marked *advertisement* in accordance with 18 U.S.C. Section 1734 solely to indicate this fact.

Received March 24, 2020; revised December 16, 2020; accepted January 13, 2021; published first January 15, 2021.

References

1. Kaufmann M, Hortobagyi GN, Goldhirsch A, Scholl S, Makris A, Valagussa P, et al. Recommendations from an international expert panel on the use of neoadjuvant (primary) systemic treatment of operable breast cancer: an update. J Clin Oncol 2006;24:1940–49.
2. Cortazar P, Zhang L, Untch M, Mehta K, Costantino JP, Wolmark N, et al. Pathological complete response and long-term clinical benefit in breast cancer: the CTNeoBC pooled analysis. Lancet 2014;384:164–72.
3. Gianni L, Eiermann W, Semiglazov V, Manikhas A, Lluch A, Tjulandin S, et al. Neoadjuvant chemotherapy with trastuzumab followed by adjuvant trastuzumab versus neoadjuvant chemotherapy alone, in patients with HER2-positive locally advanced breast cancer (the NOAH trial): a randomised controlled superiority trial with a parallel HER2-negative cohort. Lancet 2010;375:377–84.
4. Bonadonna G, Valagussa P, Brambilla C, Ferrari L. Preoperative chemotherapy in operable breast cancer. Lancet 1993;341:1485.
5. Cameron DA, Anderson EDC, Levack P, Hawkins RA, Anderson TJ, Leonard RCF, et al. Primary systemic therapy for operable breast cancer - 10-year survival data after chemotherapy and hormone therapy. Br J Cancer 1997;76:1099–105.
6. Liedtke C, Mazouni C, Hess KR, André F, Tordai A, Mejia JA, et al. Response to neoadjuvant therapy and long-term survival in patients with triple-negative breast cancer. J Clin Oncol 2008;26:1275–81.
7. Symmans WF, Peintinger F, Hatzis C, Rajan R, Kuerer H, Valero V, et al. Measurement of residual breast cancer burden to predict survival after neoadjuvant chemotherapy. J Clin Oncol 2007;25:4414–22.
8. Zhi W, Liu G, Chang C, Miao A, Zhu X, Xie L, et al. Predicting treatment response of breast cancer to neoadjuvant chemotherapy using ultrasound-guided diffuse optical tomography. Transl Oncol 2017;11:56–64.
9. Cerussi A, Hsiang D, Shah N, Mehta R, Durkin A, Butler J, et al. Predicting response to breast cancer neoadjuvant chemotherapy using diffuse optical spectroscopy. Proc Natl Acad Sci U S A 2007;104:4014–9.
10. Soliman H, Gunasekara A, Rycroft M, Zubovits J, Dent R, Spayne J, et al. Functional imaging using diffuse optical spectroscopy of neoadjuvant

chemotherapy response in women with locally advanced breast cancer. Clin Cancer Res 2010;16:2605–14.
11. Falou O, Soliman H, Sadeghi-Naini A, Iradji S, Lemon-Wong S, Zubovits J, et al. Diffuse optical spectroscopy evaluation of treatment response in women with locally advanced breast cancer receiving neoadjuvant chemotherapy. Transl Oncol 2012;5:238–46.
12. Ueda S, Roblyer D, Cerussi A, Durkin A, Leproux A, Santoro Y, et al. Baseline tumor oxygen saturation correlates with a pathologic complete response in breast cancer patients undergoing neoadjuvant chemotherapy. Cancer Res 2012; 72:4318–28.
13. Zhu Q, Wang L, Tannenbaum S, Ricci A, DeFusco P, Hegde P. Pathologic response prediction to neoadjuvant chemotherapy utilizing pretreatment near-infrared imaging parameters and tumor pathologic criteria. Breast Cancer Res 2014;16:456.
14. Lim EA, Gunther JE, Kim HK, Flexman M, Hibshoosh H, Crew K, et al. Diffuse optical tomography changes correlate with residual cancer burden after neoadjuvant chemotherapy in breast cancer patients. Breast Cancer Res Treat 2017; 162:533–40.
15. Tran WT, Gangeh MJ, Sannachi L, Chin L, Watkins E, Bruni SG, et al. Predicting breast cancer response to neoadjuvant chemotherapy using pretreatment diffuse optical spectroscopic texture analysis. Br J Cancer 2017;116:1329–39.
16. Gunther JE, Lim EA, Kim HK, Flexman M, Altoé M, Campbell JA, et al. Dynamic diffuse optical tomography for monitoring neoadjuvant chemotherapy in patients with breast cancer. Radiology 2018;287:778–86.
17. Ueda S, Yoshizawa N, Shigekawa T, Takeuchi H, Ogura H, Osaki A, et al. Near-infrared diffuse optical imaging for early prediction of breast cancer response to neoadjuvant chemotherapy: a comparative study using 18F-FDG PET/CT. J Nucl Med 2016;57:1189–95.
18. Yu Y-H, Zhu X, Mo Q-G, Cui Y. Prediction of neoadjuvant chemotherapy response using diffuse optical spectroscopy in breast cancer. Clin Transl Oncol 2018;20:524–33.
19. Liu YH, Xue LB, Yang YF, Zhao TJ, Bai Y, Zhang BY, et al. Diffuse optical spectroscopy for monitoring the responses of patients with breast cancer to neoadjuvant chemotherapy: a meta-analysis. Medicine 2018;97:e12683.
20. Tromberg BJ, Zhang Z, Leproux A, O'Sullivan TD, Cerussi AE, Carpenter PM, et al. Predicting responses to neoadjuvant chemotherapy in breast cancer: ACRIN 6691 trial of diffuse optical spectroscopic imaging. Cancer Res 2016; 76:5933–44.
21. Cochran JM, Busch DR, Leproux A, Zhang Z, O'Sullivan TD, Cerussi AE, et al. Tissue oxygen saturation predicts response to breast cancer neoadjuvant chemotherapy within 10 days of treatment. J Biomed Opt 2018;24:1–11.
22. Flexman ML, Khalil MA, Kim HK, Fong CJ, Hielscher AH, Abdi RA, et al. Digital optical tomography system for dynamic breast imaging. JBO 2011;16:076014.
23. Flexman ML, Vlachos F, Kim H-K, Hielscher AH, Sirsi SR, Borden MA, et al. Monitoring early tumor response to drug therapy with diffuse optical tomography. JBO 2012;17:016014.
24. Flexman ML, Kim HK, Gunther JE, Lim E, Alvarez MC, Desperito E, et al. Optical biomarkers for breast cancer derived from dynamic diffuse optical tomography. JBO 2013;18:096012.
25. Flexman ML, Yang Li, Bur AM, Fong CJ, Masciotti JM, Abdi RA, et al. The design and characterization of a digital optical breast cancer imaging system. In: 30th Annual International Conference of the IEEE Engineering in Medicine and Biology Society. August 20–24, 2008; Vancouver, British Columbia, Canada. p. 3735–8.
26. Kim HK, Flexman M, Yamashiro DJ, Kandel JJ, Hielscher AH. PDE-constrained multispectral imaging of tissue chromophores with the equation of radiative transfer. Biomed Opt Express 2010;1:812–24.
27. Cody DD. AAPM/RSNA physics tutorial for residents: topics in CT. Image processing in CT. Radiographics 2002;22:1255–68.
28. nlme: linear and nonlinear mixed effects models. Available from: https://CRAN.R-project.org/package=nlme.
29. Roblyer D, Ueda S, Cerussi A, Tanamai W, Durkin A, Mehta R, et al. Optical imaging of breast cancer oxyhemoglobin flare correlates with neoadjuvant chemotherapy response one day after starting treatment. Proc Natl Acad Sci U S A 2011;108:14626–31.
30. Burnside ES, Drukker K, Li H, Bonaccio E, Zuley M, Ganott M, et al. Using computer-extracted image phenotypes from tumors on breast magnetic resonance imaging to predict breast cancer pathologic stage. Cancer 2016;122: 748–57.
31. Ashraf A, Gaonkar B, Mies C, DeMichele A, Rosen M, Davatzikos C, et al. Breast DCE-MRI kinetic heterogeneity tumor markers: preliminary associations with neoadjuvant chemotherapy response. Transl Oncol 2015;8:154–62.
32. Wu J, Gong G, Cui Y, Li R. Intratumor partitioning and texture analysis of dynamic contrast-enhanced (DCE)-MRI identifies relevant tumor subregions to predict pathological response of breast cancer to neoadjuvant chemotherapy. J Magn Reson Imaging 2016;44:1107–15.
33. Kim J-H, Ko ES, Lim Y, Lee KS, Han B-K, Ko EY, et al. Breast cancer heterogeneity: MR imaging texture analysis and survival outcomes. Radiology 2016;282:665–75.
34. Braman NM, Etesami M, Prasanna P, Dubchuk C, Gilmore H, Tiwari P, et al. Intratumoral and peritumoral radiomics for the pretreatment prediction of pathological complete response to neoadjuvant chemotherapy based on breast DCE-MRI. Breast Cancer Res 2017;19:57.
35. Ku YJ, Kim HH, Cha JH, Shin HJ, Baek SH, Lee HJ, et al. Correlation between MRI and the level of tumor-infiltrating lymphocytes in patients with triple-negative breast cancer. AJR Am J Roentgenol 2016;207:1146–51.